Roles of glutamates and metal ions in a rationally designed nitric oxide reductase based on myoglobin

Ying-Wu Lin[a,2], Natasha Yeung[a], Yi-Gui Gao[b], Kyle D. Miner[c], Shiliang Tian[a], Howard Robinson[d], and Yi Lu[a,c,1]

[a]Department of Chemistry, [b]George L. Clark X-Ray Facility and 3M Materials Laboratory, and[c]Department of Biochemistry, University of Illinois at Urbana-Champaign, Urbana, IL 61801; and [d]Department of Biology, Brookhaven National Laboratory, Upton, NY 11973

Edited by Harry B. Gray, California Institute of Technology, Pasadena, CA, and approved April 1, 2010 (received for review January 14, 2010)

A structural and functional model of bacterial nitric oxide reductase (NOR) has been designed by introducing two glutamates (Glu) and three histidines (His) in sperm whale myoglobin. X-ray structural data indicate that the three His and one Glu (V68E) residues bind iron, mimicking the putative Fe_B site in NOR, while the second Glu (I107E) interacts with a water molecule and forms a hydrogen bonding network in the designed protein. Unlike the first Glu (V68E), which lowered the heme reduction potential by ~110 mV, the second Glu has little effect on the heme potential, suggesting that the negatively charged Glu has a different role in redox tuning. More importantly, introducing the second Glu resulted in a ~100% increase in NOR activity, suggesting the importance of a hydrogen bonding network in facilitating proton delivery during NOR reactivity. In addition, EPR and X-ray structural studies indicate that the designed protein binds iron, copper, or zinc in the Fe_B site, each with different effects on the structures and NOR activities, suggesting that both redox activity and an intermediate five-coordinate heme-NO species are important for high NOR activity. The designed protein offers an excellent model for NOR and demonstrates the power of using designed proteins as a simpler and more well-defined system to address important chemical and biological issues.

biomimetic models | heme-copper oxidase | metalloprotein | protein design | protein engineering

Rational design of proteins that mimic both structure and function of more complex native enzymes has been a long sought-after goal, as the process is an ultimate test of our knowledge and an excellent means to develop advanced biocatalysts (1–3). Although designed proteins that model the structure of native enzymes have been known for a while (4–10), successful designs of proteins that mimic both the structure and function of native enzymes have been reported only recently (11–16). While being able to design such functional proteins is laudable, the impact of such an achievement would be greater if the designed proteins can be used to address fundamental issues in chemistry and biology that are difficult to tackle by other methods. One primary example is the roles of conserved glutamates and metal ions in bacterial nitric oxide reductase (NOR) (17–19).

NO is critical for all life (20). Bacterial denitrification is a crucial part of the nitrogen cycle in nature that involves a four-step, five-electron reduction of nitrate (NO_3^-) to dinitrogen (N_2) (17, 19). Bacterial NOR is a membrane-bound protein that catalyzes one step of this process, namely, the two-electron reduction of NO to N_2O (17, 19). With no crystal or solution structure available for bacterial NOR to date, sequence alignments and homology modeling (21, 22) have indicated that NOR is structurally homologous to the largest subunit (subunit I) of heme-copper oxidases (HCOs) (23), enzymes that catalyze reduction of O_2 to water. The active sites of both NOR and HCO contain a proximal histidine-coordinated heme and a distal three histidine-coordinated metal center. However, the metal center in HCOs is occupied by a copper (called Cu_B), whereas a nonheme iron is present in NOR (called Fe_B) (23, 24). In addition, two conserved glutamates, shown by modeling to be close to the Fe_B site (21, 22), are found to be essential for NOR activity (24, 25). Some members of HCOs such as cytochrome cbb_3 oxidase display NOR activity (26–28), although the activity is ~50-fold lower than native NOR (26). Therefore, it is important to elucidate the structural features, specifically the roles of the conserved glutamates close to the Fe_B site and metal ions (copper vs. iron), responsible for the reduction of NO to N_2O.

To address these issues, biochemical and biophysical studies of native NOR and its variants have been carried out (24, 25, 29–37). For example, Richardson and coworkers investigated the effects of amino acid substitutions of the five conserved glutamates (E122 and E125 presumed to face the periplasm and E198, E202, and E267 located in the interior of the membrane, close to the catalytic site) in the catalytic subunit of *Paracoccus denitrificans*, NorB. The E122A, E125A, E198A, and E267A variants were inactive, indicating that these four glutamates are crucial for NOR activity (24, 25, 32, 33). On the other hand, Reimann et al. constructed a 3D model of NorB using homology modeling with the structures of HCOs as templates and suggested a plausible pathway consisting of these conserved glutamates for proton delivery (22). Despite these successes, the roles of the conserved glutamates and metal ions still remain to be fully elucidated, partly because of the difficulty in obtaining native NOR in high yield and the lack of a 3D structure. Even if these problems are resolved, it is still difficult to replace iron in the native Fe_B site with other metal ions, and spectroscopic studies of native NOR are often complicated by the presence of other metal cofactors (e.g., low-spin heme).

To overcome these limitations, a number of synthetic models of NOR using small organic molecules as ligands, have been made in which the nonheme Fe_B site can be replaced by a copper ion (17, 38–45). In addition, since these model systems lack additional metal-binding sites, spectroscopic studies are often simplified. Therefore, studies of these synthetic models have offered many insights. For example, Collman et al. showed that a fully reduced heme/nonheme Fe_B compound can react with two equivalents of NO leading to the formation of one equivalent of N_2O and a bis-ferric product (41). On the other hand, Karlin and coworkers showed that a small heme/Cu complex can efficiently lead to reductive coupling of NO to N_2O (43). However, it is also difficult to obtain the synthetic models in high yield due to the multiple steps required in chemical synthesis. Because of this limitation, no synthetic NOR model containing the two key conserved Glu residues (E198 and E267 in NOR) has been

Author contributions: Y.-W.L., N.Y., and Y.L. designed research; Y.-W.L., N.Y., Y.-G.G., K.D.M., and S.T. performed research; Y.-W.L., N.Y., Y.-G.G., K.D.M., H.R., and Y.L. analyzed data; and Y.-W.L. and Y.L. wrote the paper.

The authors declare no conflict of interest.

This article is a PNAS Direct Submission.

Data deposition: The atomic coordinates and structure factors have been deposited in the Protein Data Bank, www.pdb.org (PDB ID codes 3M38, 3M39, 3M3A, and 3M3B).

[1]To whom correspondence should be addressed. E-mail: yi-lu@illinois.edu.

[2]Present address: School of Chemistry and Chemical Engineering, University of South China, Hengyang 421001, China.

This article contains supporting information online at www.pnas.org/lookup/suppl/doi:10.1073/pnas.1000526107/-/DCSupplemental.

reported. It is also difficult to substitute different metal ions in the same metal-binding site without perturbing the site geometry and distances to the heme iron, as most ligands are not as rigid as those in native enzymes and different metal ions have different geometric and ligand donor set preferences.

We have recently designed a structural and functional protein model of bacterial NOR by engineering three histidines and one glutamate into the distal pocket of sperm whale myoglobin (swMb, L29H, F43H, H64, and V68E, named Fe_BMb) (14). Like synthetic models, this "bottom-up" approach complements the "top-down" approach of the study of native NOR in that it provides insights into whether certain "necessary" structural elements are enough to impart enzyme function. Thanks in part to recent advances in computational, molecular, and structural biology, the designed myoglobin protein model is much easier to synthesize and to crystallize than either native NOR or synthetic models. Since myoglobin has often been used for the development and calibration of numerous spectroscopic techniques (46–48), it is an ideal choice for spectroscopic studies. More importantly, the rigid protein network allows precise placement of either glutamate or metal ions in myoglobin to address their roles in NOR activity. Toward this goal, we have demonstrated that both the histidines and one of the glutamates are essential for iron binding and NO reduction activity (14). However, the role of the second Glu close to the Fe_B site and the role of different metal ions in the Fe_B site have not been addressed.

To address these important issues and to design even closer protein models of NOR, we introduced herein the second Glu to the second coordination sphere of the Fe_B site by mutating an Ile to a Glu (named I107E Fe_BMb). We show that the second Glu results in a ~100% increase in NOR activity through hydrogen bonding interactions and that the two glutamates have dramatically different effects on the heme reduction potential. Additionally, by comparing the EPR, electrochemistry, X-ray structures, and NOR activity of iron, copper, and zinc derivatives of the designed protein, we have obtained deeper insights into the roles of metal ions in NOR.

Results

Structure and Function of Fe(II)-I107E Fe_BMb. The X-ray crystal structures of heme-containing I107E Fe_BMb without metal ion in the Fe_B site and with Fe^{2+} in the Fe_B site are solved at 1.42-Å and 1.65-Å resolution, respectively (Fig. 1 *A* and *B* and Table S1). In the absence of metal ions in the Fe_B site, the structure shows a water molecule in the Fe_B site, which forms hydrogen bonds with NE2 atoms of all three His residues, both OE1 and OE2 atoms of E68, and the OE2 atom of E107 (Fig. 1*A*). Upon binding Fe^{2+}, the Fe(II)-I107E Fe_BMb structure shows that Fe^{2+} is coordinated by three His, the OE2 atom of E68, and one water molecule. Notably, a water molecule bridges Fe^{2+} in the Fe_B site and the second glutamate (E107) with a distance of 2.32 Å to the OE2 atom of E107 (Fig. 1*B*).

To probe the conformational changes of introducing the second Glu (E107), we performed a structural alignment of Fe(II)-I107E Fe_BMb and the previously reported Fe(II)-Fe_BMb (14). The comparison, shown in Fig. 2, indicates that both the polypeptide chain and the active site overlap well with each other. In addition, the two nonheme irons are located at similar positions with a 0.36-Å separation from each other. In contrast, E68 underwent a significant conformational rearrangement in the presence of E107. These observations suggest that the active site of Fe_BMb can be tuned by the formation of an extended hydrogen bonding network, resulting from the introduction of a second glutamate residue.

The binding of Fe^{2+} to deoxy I107E Fe_BMb was further monitored by EPR (Fig. 3*A*). Since deoxy myoglobin contains Fe(II) heme that exhibits no EPR signals in X-band EPR (14), we added blue copper Cu(II)-azurin (49), a redox partner of native NOR

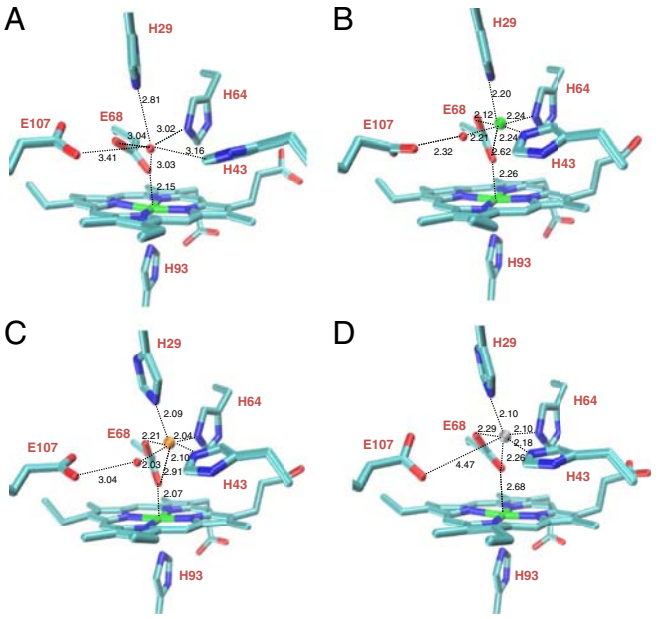

Fig. 1. Crystal structures of I107E Fe_BMb (*A*) (PDB ID code 3M38), Fe(II)-I107E Fe_BMb (*B*) (PDB ID code 3M39), Cu(II)-I107E Fe_BMb (*C*) (PDB ID code 3M3A), and Zn(II)-I107E Fe_BMb (*D*) (PDB ID code 3M3B). Water molecules, Fe(II), Cu(II), and Zn(II) are represented by red, green, orange, and gray spheres, respectively.

(19), to oxidize both the reduced heme and nonheme irons in Fe(II)-I107E Fe_BMb to EPR-active Fe(III). Upon addition of Cu(II)-azurin, the oxidation of deoxy I107E Fe_BMb resulted in EPR signals at $g = 6.12$ and 5.56, typical of a high-spin heme-Fe(III). Upon addition of Fe^{2+}, however, a decrease of the heme-Fe(III) EPR signals was observed, indicating that the Fe^{2+}, when bound to the Fe_B site and oxidized by Cu(II)-azurin, is spin-coupled to heme-Fe(III). Such a spin coupling mimics that in NOR (35, 50–53), suggesting that I107E Fe_BMb models NOR closely, at least in this respect.

To probe the role of the second Glu (E107) in NO reduction activity, we measured the yield of N_2O production by Fe(II)-I107E Fe_BMb with excess NO under one turnover conditions. We monitored N_2O formation in the headspace of the solution using GC/MS and compared this result to that of Fe(II)-Fe_BMb, which lacks the second Glu (Fig. 4). Remarkably, Fe(II)-I107E Fe_BMb displays higher activity than Fe(II)-Fe_BMb. After ~20 hr, ~24% N_2O was produced by Fe(II)-I107E Fe_BMb, in

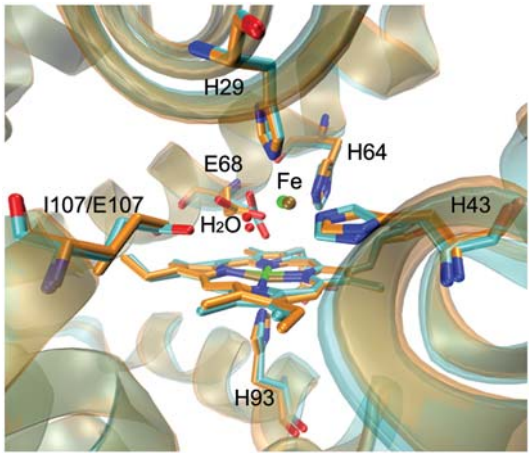

Fig. 2. Overlay of Fe(II)-I107E Fe_BMb (cyan) (PDB ID code 3M39) with Fe(II)-Fe_BMb (orange) (PDB ID code 3K9Z).

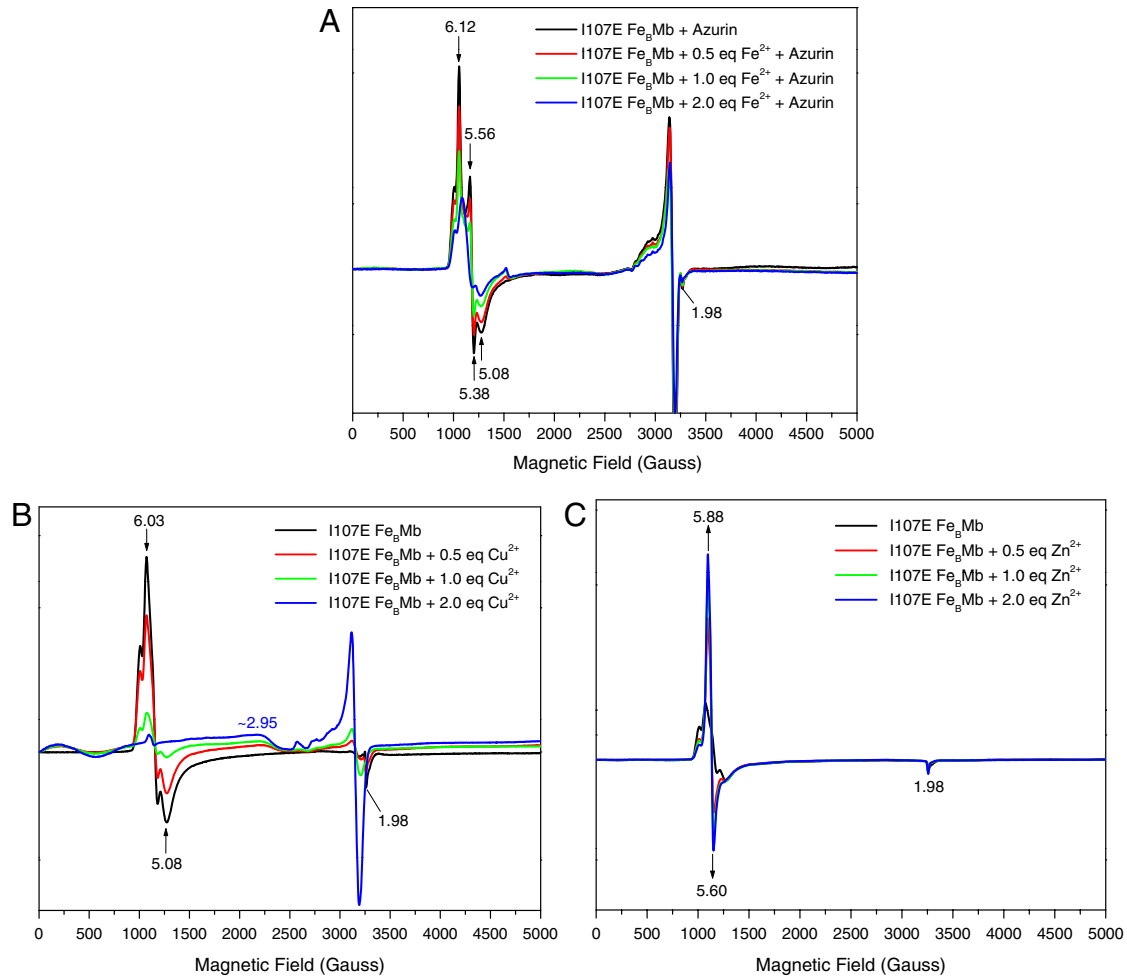

Fig. 3. EPR spectra of deoxy I107E Fe_BMb (0.5 mM protein in 50 mM Bis-Tris, pH 7.0) with increasing concentrations of Fe^{2+} in the presence of wild-type Cu(II)-azurin (*A*), and oxidized I107E Fe_BMb with Cu^{2+} (*B*) or Zn^{2+} (*C*). Spectra were collected at 4 K, 5 mW power, and 9.05 GHz.

contrast to ~10% yield for Fe(II)-Fe_BMb, strongly indicating that the second Glu plays an important role in NO reduction, likely facilitating proton uptake during NO reduction.

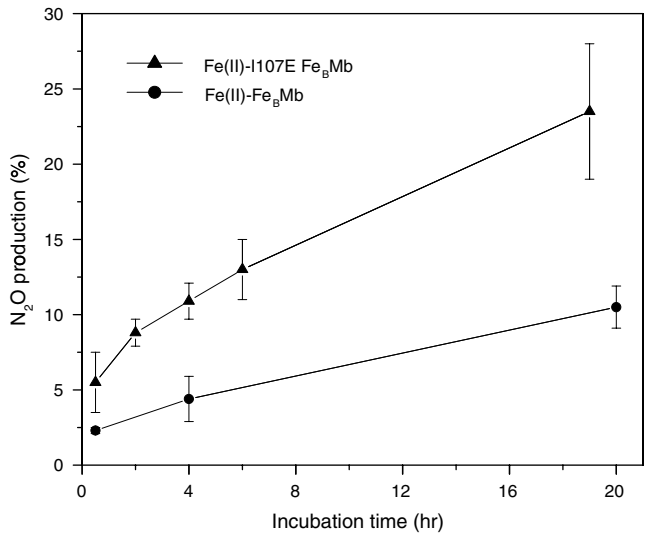

Fig. 4. Time-dependent N_2O production by Fe(II)-I107E Fe_BMb (▲) and Fe(II)-Fe_BMb (●) with ~50 eq. NO under single turnover conditions. The yield was determined by a comparison of the ratio of NO:N_2O peaks from the GC/MS chromatograms.

Other Metal Ions Binding to I107E Fe_BMb. To find out if the resting state of the protein, i.e., oxidized or met I107E Fe_BMb, can bind other metal ions, Cu^{2+} or Zn^{2+} was titrated into met I107E Fe_BMb and monitored by EPR spectroscopy (Fig. 3 *B* and *C*). In the absence of metal ions, met I107E Fe_BMb exhibited high-spin heme signals at $g = 6.03$, 5.08, and 1.98 (Fig. 3*B*, black line). Upon addition of 2 eq of Cu^{2+}, the signals at $g = 6.03$ and 5.08 decreased and a broad peak around $g = 2.95$ increased, probably due to spin coupling between heme-Fe(III) and Cu^{2+} in the Fe_B site. In contrast, addition of Zn^{2+}, a metal ion with no unpaired electrons [i.e., incapable of spin coupling to heme-Fe(III)], produced an increase in the high-spin heme signals at $g = 5.88$ and 5.60 (Fig. 3*C*), indicating that the interaction between E68 and heme iron was weakened after metal binding.

The X-ray crystal structures of I107E Fe_BMb with Cu^{2+} or Zn^{2+} in the Fe_B site were solved at 1.37-Å and 1.60-Å resolution, respectively (Fig. 1 *C* and *D* and Table S1). Compared to Fe(II)-I107E Fe_BMb (Fig. 1*B*), a similar binding site was observed for Cu(II)-I107E Fe_BMb (Fig. 1*C*), where H29, H43, and H64 coordinate to Cu^{2+} with distances of 2.09, 2.10, and 2.04 Å, respectively, slightly shorter than the corresponding distances in the Fe^{2+} structure. In comparison to Fe(II)-I107E Fe_BMb, the water bridging the Cu^{2+} and the second Glu (E107) is shifted toward Cu^{2+} in the Fe_B site (2.03 Å) with respect to E107 (3.04 Å). Interestingly, this bridging water molecule was not observed in Zn(II)-I107E Fe_BMb (Fig. 1*D*), but the two O atoms of E68 coordinate to Zn^{2+} with similar distances (2.26 Å for OE1 and 2.29 Å for OE2). The longer distance between OE1 of E68

and heme iron in the Zn-bound structure (2.68 Å) in comparison to the Cu- and Fe-bound structures, is likely the result of a weaker interaction, which is also supported by an observed increase of the high-spin heme signals in the EPR spectra upon Zn^{2+} binding (Fig. 3*C*). These results suggest I107E Fe_BMb is capable of incorporating different metal ions into its designed Fe_B site, offering an excellent opportunity to compare the role of these metal ions in the same protein scaffold.

Effect of Glutamates and Metal Ions on the Redox Potential of I107E Fe_BMb. Since EPR and X-ray structural studies indicate metal binding to I107E Fe_BMb, we used spectroelectrochemistry to measure the effects of glutamates and metal ions on the heme reduction potential. When there is no metal ion in the Fe_B site, the I107E Fe_BMb displays a reduction potential of -134 ± 3 mV vs. the normal hydrogen electrode (NHE) (Fig. S1*A*), similar to that of Fe_BMb (-158 ± 4 mV) without the I107E mutation (14). In the presence of Cu^{2+}, I107E Fe_BMb has a reduction potential (-137 ± 2 mV) (Fig. S1*B*) almost identical to that of the same protein in the absence of metal ions in the Fe_B site, indicating that copper binding to the Fe_B site has little effect on the reduction potential of the heme iron. This observation is similar to that observed for Cu^{2+} binding to Cu_BMb (Cu(II)-Cu_BMb, 80 mV vs. Cu_BMb, 77 mV) (54). On the other hand, the presence of Fe^{2+} and Zn^{2+} increased the reduction potential of I107E Fe_BMb from -134 ± 3 mV to -64 ± 3 mV vs. NHE (Fig. S1*C*) and -105 ± 2 mV vs. NHE (Fig. S1*D*), respectively. The different effects of Cu^{2+}, Fe^{2+}, and Zn^{2+} on the reduction potential of I107E-Fe_BMb indicate that these metal ions in the Fe_B site may play different roles through different coordination properties.

NOR Activity of I107E Fe_BMb in the Presence of Different Metal Ions. The NO reduction activity of I107E Fe_BMb in the presence of Fe^{2+}, Cu^{+}, or Zn^{2+} was monitored by GC/MS under single turnover conditions. When Fe(II)-I107E Fe_BMb was exposed to excess NO, N_2O could be observed to form with increased yield over time (Fig. S2). Similarly, N_2O formation was observed for Cu(I)-I107E Fe_BMb, indicating that Fe or Cu binding to the Fe_B site results in comparable NOR activities. It should be noted that because of the high solubility of N_2O (~25 mM in water at room temperature), GC/MS cannot be used to quantify the rates of NO reduction under these conditions. In contrast, no N_2O formation was observed with redox inactive Zn^{2+}, which demonstrates that redox active Fe^{2+} or Cu^{+} in the Fe_B site plays a crucial role in NO reduction.

To gain deeper insight into the process of NO reduction, EPR studies were further performed to monitor the initial process of NO reduction. In the absence of metal ions, the EPR spectrum of ferrous I107E Fe_BMb-NO shows hyperfine splitting resulting from bound NO and the proximal histidine, indicating the formation of a six-coordinate ferrous heme-NO species (Fig. 5, top line). After incubation of Fe(II)-I107E Fe_BMb with excess NO, a distinct three-line hyperfine structure appears at 15 min (Fig. 5*A*), suggesting the formation of a five-coordinate ferrous heme-NO species as a result of cleavage of the proximal His-Fe heme bond (55). A three-line hyperfine structure was also observed for Cu^{+} and Zn^{2+}, except that the signal intensity is lower with Cu(I)-I107E Fe_BMb-NO (Fig. 5*B*) and more pronounced in Zn(II)-I107E Fe_BMb-NO (Fig. 5*C*). The lower intensity of the three-line hyperfine structure for Cu(I)-I107E Fe_BMb-NO suggests the major species formed is a six-coordinate ferric heme-NO complex, which is EPR silent (41). These differences further suggest that the metal ion in the Fe_B site plays a key role in formation of the intermediates, thereby tuning NOR activity.

Discussion

Using Rationally Designed Proteins to Address Important Issues in Chemistry and Biology. Important issues such as the roles of the conserved glutamates and nonheme Fe_B in NOR have been previously addressed using biochemical and biophysical studies or biomimetic modeling (24, 25, 27–37, 45, 56, 57). As a complementary approach, rational protein design, using small, easy-to-produce and well-characterized proteins such as myoglobin, offers a powerful method with which to gain insights into more complex native enzymes such as NOR (14). Similar to synthetic models (41, 43), the metal ion at the putative Fe_B site in the protein model can be substituted freely. Better yet, Glu residues can be placed at precise locations in the protein, including the secondary coordination sphere, due to its rigid network. By carefully choosing a suitable protein template, rational protein design could be generally applied to address other important issues in chemistry and biology.

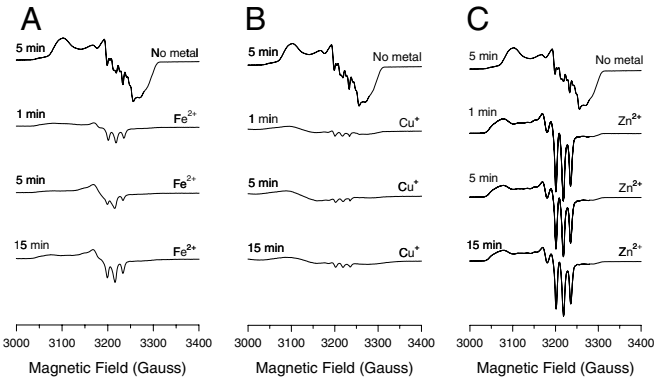

Fig. 5. EPR spectra of deoxy I107E Fe_BMb (0.5 mM) with no metal bound in the presence of NO after 5 min (top line), with 2 eq Fe^{2+} (*A*), Cu^{+} (*B*), or Zn^{2+} (*C*) incubated with excess NO (~200 eq) for 1, 5, and 15 min. Spectra were collected in 50 mM Bis-Tris pH 7.0 at 30 K, 0.2 mW power, and 9.05 GHz.

The Roles of Glutamates. Although two conserved glutamates (E198 and E267) are known to be crucial for NOR activity (24, 25), their roles are not well defined (18, 19). In a previous study (14), we demonstrated that one Glu, E68, is important for both iron binding and NOR activity of Fe_BMb. The crystal structures of both Fe(II)-Fe_BMb and Fe(II)-I107E Fe_BMb show that one O atom of E68 directly coordinates to Fe_B (Fig. 2). In synthetic models of NOR, it has also been found that the presence of a glutamic acid mimic significantly increases the stability of iron binding to the Fe_B site (40). Furthermore, a theoretical study by Blomberg et al. (58) showed that a model with an Fe_B coordinated by three histidines, one glutamate, and one water molecule provides an energetically feasible reaction mechanism of NO reduction. However, the structural model of NOR constructed recently by Reimann et al. (22) shows that the closest conserved Glu (E267) still has its carboxylate O atom 7 Å away from Fe_B, which suggests that Glu may not bind to Fe_B in native NOR. One interesting finding from our study is that the Glu (E68) underwent a significant conformational rearrangement in the presence of another Glu (E107) (Fig. 2). Therefore, the Fe_BMb provides a viable model of NOR that is consistent with Blomberg's model, but cannot rule out Reimann's model due to possible conformation changes.

While the role of the first Glu is still uncertain until a 3D structure of NOR in its active form is available, the role of the second Glu is even less defined. We address this question by introducing a second Glu (E107) to Fe_BMb. The crystal structures shown in Fig. 1 indicate that E107 interacts with a water molecule and forms a hydrogen bonding network in both Fe(II)-I107E Fe_BMb and Cu(II)-I107E Fe_BMb. Interestingly, although a similar water molecule was observed in the active site of Fe(II)-Fe_BMb (Fig. 2), activity assay data indicate that the presence of E107 in Fe(II)-I107E Fe_BMb increases NOR activity by ~100%

(Fig. 4), suggesting that the second Glu may potentionally play a role in providing one of the protons during reduction of NO to N_2O. Although free Glu outside a protein has a $pK_a \sim 4.3$, the studies of native NOR showed that the pK_a of its Glu close to the active site has a value of ~6.6 (22, 25, 33). The hydrogen binding network in our protein models may contribute to the fine-tuning of the Glu pK_a to be more neutral, similar to that in NOR. Moreover, it is interesting that Cu(I)-I107E Fe_BMb also shows NOR activity, which provides an interesting protein model of HCOs with NOR function (26–28), even though Glu residues are not conserved in native HCOs.

Additionally, spectroelectrochemical studies showed that the reduction potential of I107E Fe_BMb with no metal ion in the Fe_B site is similar to that of Fe_BMb, but much lower than that of Cu_BMb (77 mV) (54), which contains the same three His, but no Glu in the metal-binding site above the heme. Since both Fe_BMb and I107E Fe_BMb contain the V68E mutation that has been shown to decrease the heme reduction potential of native myoglobin from 59 mV to −137 mV (59), it is likely that the introduction of a negatively charged Glu close to the heme group is what is responsible for the dramatically lower heme redox potential. A conserved glutamate, predicted to be located near the catalytic heme b_3 in NOR, was proposed to be responsible for a ~260-mV decrease in reduction potential (60 mV) in comparison to the other two heme centers, heme *b* (345 mV) and heme *c* (310 mV) (60). Our Fe_BMb and I107E Fe_BMb models mimic this feature of NOR. Notably, although introduction of the first Glu (E68) lowered the heme potential by ~110 mV (14), introduction of the second Glu via the I107E mutation did not result in a significant difference in the heme reduction potential, suggesting that the effect of the two conserved Glu residues in NOR on heme reduction potential is not additive, with the effects highly dependent on the location of the Glu.

The Roles of Metal Ions. The roles of metal ions in NOR are another important question as iron is found in the native Fe_B site and HCO employs copper at the corresponding Cu_B site. With different metal ions in the Fe_B site, the crystal structures clearly show the heme and nonheme dinuclear center existing in different local environments (Fig. 1). Although a similar hydrogen bond network is formed in both Fe(II)-I107E Fe_BMb and Cu(II)-I107E Fe_BMb, the conformation of E68 and E107 with respect to the nonheme metal center and heme iron is different from each other. Moreover, the coordination geometry differs significantly with Zn^{2+} in the Fe_B site. A hydrogen bond is absent from the Zn crystal structure, but both the O atoms of E68 act as metal-binding ligands. These observations demonstrate that the identity of the metal ion in the Fe_B site can tune the active site through their interactions with the His and Glu ligands, resulting in formation of different coordination geometries with different hydrogen bonds.

In addition to structural fine-tuning, the metal ion at the Fe_B site can also tune the heme iron reduction potential in I107E Fe_BMb. Spectroelectrochemical studies showed that the binding of Fe^{2+} or Zn^{2+} results in an increase in the heme reduction potential by ~70 mV and ~30 mV, respectively (Fig. S1). In the case of Cu(II)-I107E Fe_BMb, the crystal structure shows that OE1 of E68 is closer to the heme iron (2.07 Å) (Fig. 1*C*) than its metal-free form (2.15 Å) (Fig. 1*A*). The stronger interaction from the negatively charged E68 could offset the effect of positively charged Cu^{2+} binding, resulting in similar reduction potentials observed for Cu(II)-I107E Fe_BMb and I107E Fe_BMb.

In a previous study (61), EPR data showed that during NO reduction, the binding of Cu^+ to the Cu_B site of Cu_BMb can weaken the proximal heme Fe-His bond, while complete cleavage of the heme Fe-His bond occurred when Zn^{2+} was bound to Cu_BMb-NO. In this study, we observed that a five-coordinate heme-NO species was formed with Fe^{2+}, Cu^+, or Zn^{2+} bound to the Fe_B site of I107E Fe_BMb (Fig. 5). Significantly, a five-coordinate heme-NO species has also been observed for both NOR (30, 31, 35) and the member of the HCO family with the highest NO reduction activity, cytochrome cbb_3 oxidases (26, 62). However, this species was not observed for Fe(II)-Fe_BMb-NO and Cu(I)-Fe_BMb-NO, which lack the second Glu (E107). In both these cases, the proximal heme Fe-His bond was only weakened, as indicated by a decrease of the nine-line hyperfine splitting signals in the EPR spectra (Fig. S3). These observations suggest that formation of a five-coordinate heme-NO species may play an important role in NOR reactivity.

Conclusions

We have successfully designed a structural and functional model of NOR, by introducing a second glutamate in the vicinity of the Fe_B site, named I107E Fe_BMb. This protein model mimics native NOR more closely by bearing the structural feature of three histidines and two glutamates in the Fe_B site, as predicted for native NOR. We have demonstrated that the two glutamates can play different roles in NO reduction activity; namely, one acts as a ligand to Fe_B (E68), and the other acts as a proton transfer group (E107). Furthermore, by substituting different metal ions into the nonheme metal site, we have demonstrated that Fe_B plays crucial roles in fine-tuning the active site by donating electrons and by mediating the formation of a five-coordinate heme-NO intermediate during NO reduction. In the absence of a crystal structure for native NOR, this study offers an ideal protein model and provides valuable structural as well as mechanistic information for native NOR.

Materials and Methods

Protein Preparation. I107E Fe_BMb (swMb L29H/F43H/V68E/I107E) was constructed, expressed, and purified using the procedure described previously (14). The purity and identity were confirmed by SDS-PAGE and electrospray ionized MS: observed: 17, 392 ± 1 Da; calculated: 17,391 Da.

EPR Spectroscopy. EPR spectra were recorded on a Bruker ESP 300 equipped with an Oxford liquid helium cryostat and an ITC4 temperature controller. The samples of met I107E Fe_BMb, Cu(II)-, or Zn(II)-I107E Fe_BMb were prepared as described previously (14). The samples of NO-bound deoxy I107E Fe_BMb, Cu(I)-, Fe(II)-, or Zn(II)-I107E Fe_BMb were prepared by injecting 1 mL of purified NO gas into the EPR tube containing 300 μL of protein (0.5 mM, 10% glycerol, in 50 mM Bis-Tris pH 7.0). The samples were then flash frozen in liquid N_2 after incubation for 1, 5, or 15 min. The molar extinction coefficient of the Soret band of I107E Fe_BMb at 406 nm (175 $mM^{-1} \cdot cm^{-1}$), calculated using the standard hemochromagen method (63), was used to determine protein concentration. The metal sources of Cu(I), Cu(II), Zn(II), and Fe(II) were $[(CH_3CN)_4Cu]PF_6$, $CuSO_4$, $ZnSO_4 \cdot 7H_2O$, and $FeCl_2$, respectively.

Spectroelectrochemical Measurements. Protein reduction potentials were measured using an optically transparent thin layer electrode as previously described (64). The potential of the working electrode was applied in the positive direction for deoxy I107E Fe_BMb with Fe^{2+} and in the negative direction for metal free and with Cu^{2+} or Zn^{2+}. Other procedures are the same as described previously (54).

X-Ray Crystallographic Studies. Fe(II)-I107E Fe_BMb was crystallized anaerobically in a glove box at room temperature using the conditions described for Fe(II)-Fe_BMb (14). I107E Fe_BMb, Cu(II)-, or Zn(II)-I107E Fe_BMb were crystallized aerobically. Diffraction-quality crystals were soaked in a cryoprotectant solution of 30% PEG 400 and flash frozen in liquid nitrogen. Diffraction data were collected at the Brookhaven National Lab Synchrotron Light Source X12C beamline. The crystal structure was solved using the same method as for Fe(II)-Fe_BMb (14).

NOR Activity Assay. NO reduction was monitored by GC/MS. The protein was reduced to the deoxy form by excess dithionite that was removed with a size-exclusion column (PD-10). Then 2 eq metal, Cu(I), Fe(II), or Zn(II), was added to the protein solution (0.6 mM, 3 mL in 50 mM Bis-Tris buffer, pH 7.0). The samples were prepared anaerobically in a glove box. Purified NO

gas was injected into the head space of the reaction flask with the molar ratio of NO:protein ≈ 50:1. Other procedures are the same as described previously (14, 61).

ACKNOWLEDGMENTS. We thank Dr. Mark J. Nilges for help with EPR analysis, and Furong Sun and Beth D. Eves for aiding in GC/MS data collection. This work was supported by NIH Grant GM062211.

1. Lu Y, Yeung N, Sieracki N, Marshall NM (2009) Design of functional metalloproteins. *Nature* 460:855–862.
2. Nanda V, Koder RL (2010) Designing artificial enzymes by intuition and computation. *Nat Chem* 2:15–24.
3. Gray HB (2003) Biological inorganic chemistry at the beginning of the 21st century. *Proc Natl Acad Sci USA* 100:3563–3568.
4. Regan L, DeGrado WF (1988) Characterization of a helical protein designed from first principles. *Science* 241:976–978.
5. Hecht MH, Richardson JS, Richardson DC, Ogden RC (1990) De novo design, expression, and characterization of Felix: A four-helix bundle protein of native-like sequence. *Science* 249:884–891.
6. Robertson DE, et al. (1994) Design and synthesis of multi-heme proteins. *Nature* 368:425–432.
7. Lu Y, Valentine JS (1997) Engineering metal-binding sites in proteins. *Curr Opin Struct Biol* 7:495–500.
8. Reedy CJ, Gibney BR (2004) Heme protein assemblies. *Chem Rev* 104:617–649.
9. Watanabe Y, Hayashi T (2005) Functionalization of myoglobin. *Prog Inorg Chem* 54:449–493.
10. Ghosh D, Pecoraro VL (2005) Probing metal-protein interactions using a de novo design approach. *Curr Opin Chem Biol* 9:97–103.
11. Kaplan J, DeGrado WF (2004) De novo design of catalytic proteins. *Proc Natl Acad Sci USA* 101:11566–11570.
12. Kang SG, Saven JG (2007) Computational protein design: Structure, function and combinatorial diversity. *Curr Opin Chem Biol* 11:329–334.
13. Jiang L, et al. (2008) De novo computational design of retro-aldol enzymes. *Science* 319:1387–1391.
14. Yeung N, et al. (2009) Rational design of a structural and functional nitric oxide reductase. *Nature* 462:1079–1082.
15. Koder RL, et al. (2009) Design and engineering of an O_2 transport protein. *Nature* 458:305–309.
16. Heinisch T, Ward TR (2010) Design strategies for the creation of artifical metalloenzymes. *Curr Opin Chem Biol* 14:184–199.
17. Wasser IM, de Vries S, Moënne-Loccoz P, Schröder I, Karlin KD (2002) Nitric oxide in biological denitrification: Fe/Cu metalloenzyme and metal complex NOx redox chemistry. *Chem Rev* 102:1201–1234.
18. Yeung N, Lu Y (2008) One heme, diverse functions: Using biosynthetic myoglobin models to gain insights into heme-copper oxidases and nitric oxide reductases. *Chem Biodivers* 5:1437–1454.
19. Watmough NJ, Field SJ, Hughes RJL, Richardson DJ (2009) The bacterial respiratory nitric oxide reductase. *Biochem Soc Trans* 37:392–399.
20. Cary SPL, Winger JA, Derbyshire ER, Marletta MA (2006) Nitric oxide signaling: No longer simply on or off. *Trends Biochem Sci* 31:231–239.
21. Sakurai N, Sakurai T (1998) Genomic DNA cloning of the region encoding nitric oxide reductase in paracoccus halodenitrificans and a structure model relevant to cytochrome oxidase. *Biochem Biophys Res Commun* 243:400–406.
22. Reimann J, Flock U, Lepp H, Honigmann A, Ädelroth P (2007) A pathway for protons in nitric oxide reductase from paracoccus denitrificans. *Biochim Biophys Acta* 1767:362–373.
23. Pereira MM, Sousa FL, Verissimo AF, Teixeira M (2008) Looking for the minimum common denominator in haem-copper oxygen reductases: Towards a unified catalytic mechanism. *Biochim Biophys Acta* 1777:929–934.
24. Butland G, Spiro S, Watmough NJ, Richardson DJ (2001) Two conserved glutamates in the bacterial nitric oxide reductase are essential for activity but not assembly of the enzyme. *J Bacteriol* 183:189–199.
25. Flock U, Lachmann P, Reimann J, Watmough NJ, Äedelroth P (2009) Exploring the terminal region of the proton pathway in the bacterial nitric oxide reductase. *J Inorg Biochem* 103:845–850.
26. Forte E, et al. (2001) The cytochrome cbb3 from pseudomonas stutzeri displays nitric oxide reductase activity. *Eur J Biochem* 268:6486–6490.
27. Huang Y, Reimann J, Lepp H, Drici N, Ädelroth P (2008) Vectorial proton transfer coupled to reduction of O2 and NO by a heme-copper oxidase. *Proc Natl Acad Sci USA* 105:20257–20262.
28. Hayashi T, et al. (2009) Accommodation of two diatomic molecules in cytochrome bo3: Insights into NO reductase activity in terminal oxidases. *Biochemistry* 48:883–890.
29. Moënne-Loccoz P (2007) Spectroscopic characterization of heme iron-nitrosyl species and their role in NO reductase mechanisms in diiron proteins. *Nat Prod Rep* 24:610–620.
30. Moënne-Loccoz P, de Vries S (1998) Structural characterization of the catalytic high-spin heme b of nitric oxide reductase: A resonance raman study. *J Am Chem Soc* 120:5147–5152.
31. Sakurai T, Sakurai N, Matsumoto H, Hirota S, Yamauchi O (1998) Roles of four iron centers in paracoccus halodenitrificans nitric oxide reductase. *Biochem Biophys Res Commun* 251:248–251.
32. Thorndycroft FH, Butland G, Richardson DJ, Watmough NJ (2007) A new assay for nitric oxide reductase reveals two conserved glutamate residues form the entrance to a proton-conducting channel in the bacterial enzyme. *Biochem J* 401:111–119.
33. Flock U, et al. (2008) Defining the proton entry point in the bacterial respiratory nitric-oxide reductase. *J Biol Chem* 283:3839–3845.
34. Hendriks JHM, Jasaitis A, Saraste M, Verkhovsky MI (2002) Proton and electron pathways in the bacterial nitric oxide reductase. *Biochemistry* 41:2331–2340.
35. Kumita H, et al. (2004) NO reduction by nitric-oxide reductase from denitrifying bacterium pseudomonas aeruginosa: Characterization of reaction intermediates that appear in the single turnover cycle. *J Biol Chem* 279:55247–55254.
36. Pinakoulaki E, Varotsis C (2008) Resonance raman spectroscopy of nitric oxide reductase and cbb3 heme-copper oxidase. *J Phys Chem B* 112:1851–1857.
37. Kapetanaki SM, et al. (2008) Ultrafast ligand binding dynamics in the active site of native bacterial nitric oxide reductase. *Biochim Biophys Acta* 1777:919–924.
38. Wasser IM, et al. (2004) Synthesis and spectroscopy of m-oxo (O2-)-bridged Heme/Non-heme diiron complexes: Models for the active site of nitric oxide reductase. *Inorg Chem* 43:651–662.
39. Wasser IM, Huang H, Moënne-Loccoz P, Karlin KD (2005) Heme/Non-heme diiron(II) complexes and O_2, CO, and NO adducts as reduced and substrate-bound models for the active site of bacterial nitric oxide reductase. *J Am Chem Soc* 127:3310–3320.
40. Collman JP, Yan Y, Lei J, Dinolfo PH (2006) Active-site models of bacterial nitric oxide reductase featuring tris-histidyl and glutamic acid mimics: Influence of a carboxylate ligand on Fe_B binding and the heme Fe/Fe_B redox potential. *Inorg Chem* 45:7581–7583.
41. Collman JP, et al. (2008) A functional nitric oxide reductase model. *Proc Natl Acad Sci USA* 105:15660–15665.
42. Collman JP, et al. (2008) Intermediates involved in the two electron reduction of NO to N_2O by a functional synthetic model of heme containing bacterial NO reductase. *J Am Chem Soc* 130:16498–16499.
43. Wang J, Schopfer MP, Sarjeant Amy AN, Karlin KD (2009) Heme-copper assembly mediated reductive coupling of nitrogen monoxide (*NO). *J Am Chem Soc* 131:450–451.
44. Liu J, Naruta Y, Tani F (2005) A functional model of the cytochrome c oxidase active site: Unique conversion of a heme-m-peroxo-CuII intermediate into heme-superoxo/CuI. *Angew Chem Int Edit* 44:1836–1840.
45. Ghiladi RA, et al. (2005) Heme-copper/dioxygen adduct formation relevant to cytochrome c oxidase: Spectroscopic characterization of $[(6L)FeIII\text{-}(O_2^{2-})\text{-}CuII]+$. *J Biol Inorg Chem* 10:63–77.
46. Sage JT (1997) Myoglobin and CO: Structure, energetics, and disorder. *J Biol Inorg Chem* 2:537–543.
47. Sigman JA, Kim HK, Zhao X, Carey JR, Lu Y (2003) The role of copper and protons in heme-copper oxidases: Kinetic study of an engineered heme-copper center in myoglobin. *Proc Natl Acad Sci USA* 100:3629–3634.
48. Davydov R, Hoffman BM (2008) EPR and ENDOR studies of fe(II) hemoproteins reduced and oxidized at 77 K. *J Biol Inorg Chem* 13:357–369.
49. Marshall NM, et al. (2009) Rationally tuning the reduction potential of a single cupredoxin beyond the natural range. *Nature* 462:113–116.
50. Girsch P, de Vries S (1997) Purification and initial kinetic and spectroscopic characterization of NO reductase from paracoccus denitrificans. *Biochim Biophys Acta* 1318:202–216.
51. Sakurai N, Sakurai T (1997) Isolation and characterization of nitric oxide reductase from paracoccus halodenitrificans. *Biochemistry* 36:13809–13815.
52. Hendriks J, et al. (1998) The active site of the bacterial nitric oxide reductase is a dinuclear iron center. *Biochemistry* 37:13102–13109.
53. Moënne-Loccoz P, et al. (2000) Nitric oxide reductase from paracoccus denitrificans contains an oxo-bridged Heme/Non-heme diiron center. *J Am Chem Soc* 122:9344–9345.
54. Zhao X, Yeung N, Wang Z, Guo Z, Lu Y (2005) Effects of metal ions in the CuB center on the redox properties of heme in heme-copper oxidases: Spectroelectrochemical studies of an engineered heme-copper center in myoglobin. *Biochemistry* 44:1210–1214.
55. Decatur SM, et al. (1996) Trans effects in nitric oxide binding to myoglobin cavity mutant H93G. *Biochemistry* 35:4939–4944.
56. Pervitsky D, Immoos C, van der Veer W, Farmer PJ (2007) Photolysis of the HNO adduct of myoglobin: Transient generation of the aminoxyl radical. *J Am Chem Soc* 129:9590–9591.
57. Berto TC, Praneeth VKK, Goodrich LE, Lehnert N (2009) Iron-porphyrin NO complexes with covalently attached N-donor ligands: Formation of a stable six-coordinate species in solution. *J Am Chem Soc* 131:17116–17126.
58. Blomberg LM, Blomberg MRA, Siegbahn PEM (2006) Reduction of nitric oxide in bacterial nitric oxide reductase-a theoretical model study. *Biochim Biophys Acta* 1757:240–252.
59. Varadarajan R, Zewert TE, Gray HB, Boxer SG (1989) Effects of buried ionizable amino acids on the reduction potential of recombinant myoglobin. *Science* 243:69–72.
60. Grönberg KLC, et al. (1999) A low-redox potential heme in the dinuclear center of bacterial nitric oxide reductase: Implications for the evolution of energy-conserving heme-copper oxidases. *Biochemistry* 38:13780–13786.
61. Zhao X, Yeung N, Russell BS, Garner DK, Lu Y (2006) Catalytic reduction of NO to N_2O by a designed heme copper center in myoglobin: Implications for the role of metal ions. *J Am Chem Soc* 128:6766–6767.
62. Pinakoulaki E, Stavrakis S, Urbani A, Varotsis C (2002) Resonance raman detection of a ferrous five-coordinate nitrosylheme b3 complex in cytochrome cbb3 oxidase from pseudomonas stutzeri. *J Am Chem Soc* 124:9378–9379.
63. Morrison M, Horie S (1965) Determination of heme a concentration in cytochrome preparations by hemochromogen method. *Anal Biochem* 12:77–82.
64. Taboy CH, Bonaventura C, Crumbliss AL (2002) Anaerobic oxidations of myoglobin and hemoglobin by spectroelectrochemistry. *Method Enzymol* 353:187–209.